Aeroacoustic modeling of a low Reynolds number rotor in the wake of a cylindrical beam

Romain Gojon, Emma Vella, Nicolas Doué, Hélène Parisot-Dupuis, Bertrand Mellot, Thierry Jardin

25-29 August 2024
inter.noise
NANTES FRANCE

Aeroacoustic modeling of a low Reynolds number rotor in the wake of a cylindrical beam

Romain Gojon [1], Emma Vella, Nicolas Doué, Hélène Parisot Dupuis, Bertrand Mellot, and Thierry Jardin
ISAE-SUPAERO, Université de Toulouse
10 av. Edouard Belin, 31400, Toulouse, FRANCE

ABSTRACT

In micro air vehicles, low Reynolds number rotors operating in close proximity to the fuselage raises the question of interaction noise as a prominent acoustic source. The underlying noise generation mechanisms can be either the unsteady loading on the blade due to the presence of a nearby surface, the unsteady loading on the fuselage, and/or the diffraction of one source by the other surface. This paper proposes to comprehensively explore those interaction noise generation mechanisms, employing numerical simulations, experimental approaches, and analytical modelling. The focus is on scenarios where a low Reynolds number rotor is located in the wake of a cylindrical beam, and oppositely when the beam is in the wake of the rotor. In both scenarios, it is observed experimentally that the amplitudes of the BPF harmonics are increased with respect to that obtained without beam. This increase is higher when the rotor is in the wake of the beam compared to when the beam is in the wake of the rotor. The numerical simulation is shown to reproduce quite well the envelope of the amplitudes of the BPF harmonics obtained experimentally in both scenarios. Interestingly, by applying Ffowcs-Williams and Hawkings analogy on elementary surfaces, and not on the whole rotor-beam surface, the main sound generation mechanism was found to be the unsteady loading on the beam in both scenarios. Finally, an analytical modeling of the noise source mechanism is performed and compared with experimental and numerical results, showing good agreement when the beam is in the wake of the rotor, but not when the rotor is in the wake of the beam, suggesting another mechanism at play in the later case.

1. INTRODUCTION

Quadcopter unmanned air vehicles (UAVs) are being increasingly used in civilian and military fields due to their versatility and cost-effectiveness. They serve various purposes such as filming for the cinema industry, inspecting infrastructure like dams, and conducting reconnaissance missions. However, this rise in UAV usage may exacerbate noise pollution, prompting aviation agencies to implement stricter certification standards to safeguard civilians from UAV noise. Consequently, comprehending UAV noise generation mechanisms becomes crucial for designing UAVs compliant with these standards. In quadcopter UAVs, primary noise sources include rotor noise and interactions between rotors and frames.

The study of rotor noise began in the first half of the 20th century, with Gutin [1] investigating rotor noise at blade passing frequency (BPF) and its harmonics. Williams [2] extended this theory

[1] romain.gojon@isae-supaero.fr

to consider quadrupole noise sources, which are significant for high Mach number propellers. Subsequent studies, such as those by George [3] and Brentner [4], primarily focused on high Reynolds number rotors like helicopter rotors, limiting direct applicability to quadcopter UAVs operating at lower Reynolds and Mach numbers.

Recent experimental and numerical investigations have focused on low Reynolds and low Mach number hovering isolated rotors. Zawodny et al. [5] conducted experimental analysis of small-scale off-the-shelf rotors, while Jo et al. [6] used a non-linear vortex lattice method (NLVLM) coupled with the Ffowcs-Williams and Hawkings analogy (FW-H) to study the effect of blade number on hovering rotor aeroacoustics. Serre et al. [7, 8] performed aeroacoustic optimization of hovering rotors through low-order models, showing significant noise reduction compared to conventional rotors. At TU-Delft, Grande et al. [9] experimentally studied the performance and noise emitted by low Reynolds number rotors for different advance ratios using an aeroacoustic wind tunnel. Romani et al. [10] conducted lattice-Boltzmann simulations (LBM) to understand the effects of zig-zag transition trip and its chordwise position on rotor performance and radiated noise. Additionally, Gojon et al. [11] provided an open experimental database on 3D-printed academic low Reynolds number rotors and derived scaling laws for different noise sources.

Studies have also been conducted on rotor-frame and rotor-rotor interactions. Zawodny et al. [12] investigated rotor-frame interaction noise for a two-bladed rotor, showing its dependence on frame geometry and position relative to the rotor disk plane. Wu et al. [13] analyzed tonal noise produced by a two-bladed UAV rotor operating with a cylindrical beam placed in the wake, deriving an analytical model for the radiated noise field. Roger et al. [14] studied propeller-wing interaction noise, where the propeller was located downstream of the frame element, cutting the wake. They proposed an analytical formulation for the sound emitted by this interaction at BPF harmonics. Similarly, for wind turbine applications, Cotté et al. [15] studied the tonal noise due to the interaction of a simplified three-bladed rotor and a circular tower. More complex configurations with multiple rotors and frames were also recently investigated [16–19].

In summary, while previous studies have shed light on various aspects of UAV noise generation, there remains a need for further research, particularly in understanding the influence of parameters on noise emission in rotor-frame configurations. In this paper, we report on an investigation of the noise generated by small scale rotors operating under hovering conditions and interacting with a cylindrical beam placed either upstream or downstream of the rotor, following the direction of the flow. The experimental and numerical setups are first described in section II. Then, the aerodynamics and acoustics results are presented in section III where the main noise source mechanism is unraveled. Finally, in section IV, an analytical modeling of the main acoustic source is presented and compared with numerical and experimental results.

2. EXPERIMENTAL AND NUMERICAL SETUPS

In this experimental and numerical study, we consider two different rotors in interaction with a cylindrical beam of diameter $D = 20$ mm , positioned at a distance $L = 20$ mm below the rotor disk plane. As in previous studies [20, 21], L is defined as the distance between the rotor disk plane (passing through the blades at mid-chord) and the axis of the cylindrical beam. The rotational speed of the rotors is set to 8000 RPM. The rotors feature a NACA0012 blade cross-section profile extruded in the radial direction with a constant chord of 25 mm, a constant pitch of 10° and a diameter of 200 mm. The only difference between those two rotors is that one is having a left hand pitch, permitting to produce a flow going downward, in the direction of the beam, whereas the second is characterized by a right hand pitch, leading to a flow going upward, i.e. away from the beam. Those two rotors will be labeled RD and RU, respectively.

As the experimental and numerical setups are almost identical to those used in previous studies, they are recalled briefly here, but the interested reader can find more information in corresponding references [20, 21].

2.1. Experimental setup

For this experimental campaign, the two rotors have been 3D-printed using stereolithography. They are positioned at the center of the ISAE-SUPAERO anechoic room at the top of a rotor test stand with the beam below, as it can be seen in Figure 1 for the rotor RD. The rotor is driven by means of a Faulhaber 3274G024BP4 3692 electric brushless motor, which presents low noise emissions as compared to conventional off-the-shelf motors [11]. A six-axis ATI Nano17 load cell is placed beneath the motor for measuring aerodynamic loads. A directivity antenna with 13 1/4" GRAS 40PH microphones is used to measure the farfield noise radiated 1620 mm away from the rotor center, for latitude angles θ every 10° from -60° to 60°, where 0° corresponds to the rotor disk plane. Moreover, in order to be able to study the directivity along the rotor disk plane, the test stand is positioned on a turntable so that one can rotate in azimuth the whole rotor-beam setup. With the couple directivity antenna/turntable, the almost complete spherical directivity can be investigated, only the poles ($|\theta| > 60°$) being missing. Acoustic data are acquired at a sampling frequency of 51.2 kHz, during 16 s. This experimental setup has been used and validated in several papers [11, 21, 22]. Please note that for the RU rotor, the azimuthal angle remains identical, i.e. positive angles are now in the direction of the flow.

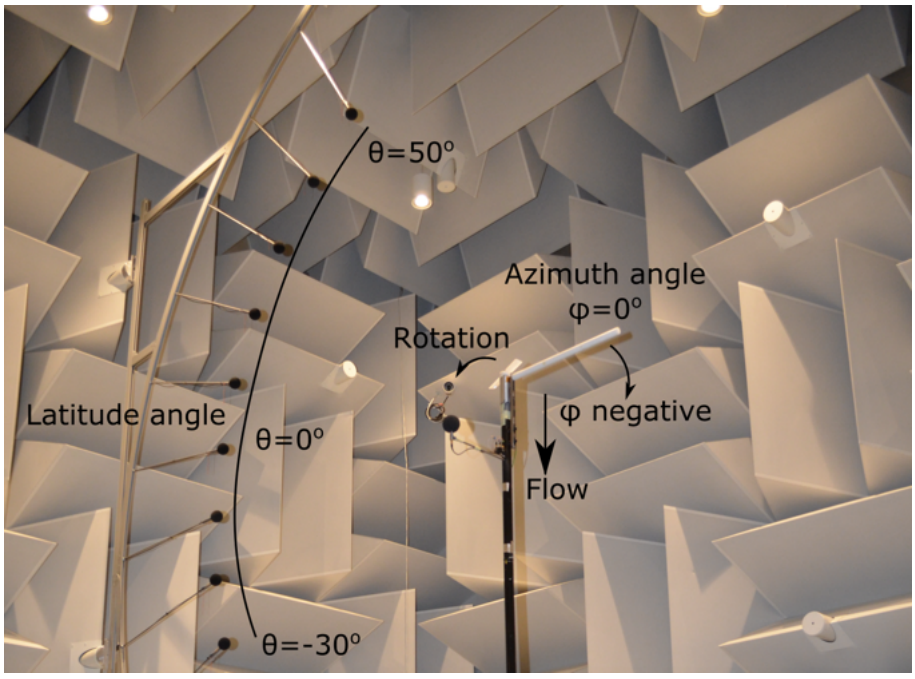

Figure 1: Photograph of the experimental setup: rotor RD in interaction with the beam.

2.2. Numerical methods and meshes

Simulations for both RD and RU rotors are performed with the CFD commercial software Fluent v2020 R1. The numerical model comprises the two blades, the hub and the beam, as shown in Figure 2 for the rotor RD. The computational domain is divided into two parts: an inner rotating volume housing notably the rotor and its hub, and an outer static volume for the beam, the mast, and the farfield boundary conditions. This division is represented by a black line in Figure 2 (right). Both volumes are meshed with polyhedral cells. Prism layers are generated at walls for boundary layers discretization, and the thickness of the first prism layer was calculated to target a Y+ value around 1. The inner and outer volumes communicate through interfaces. All walls are modelled as non-slip walls. Upstream, downstream and lateral boundaries in the outer volume are modelled as pressure inlet, pressure outlet and slip walls, respectively. The total number of cells for each

geometrical configuration is around 7 millions.

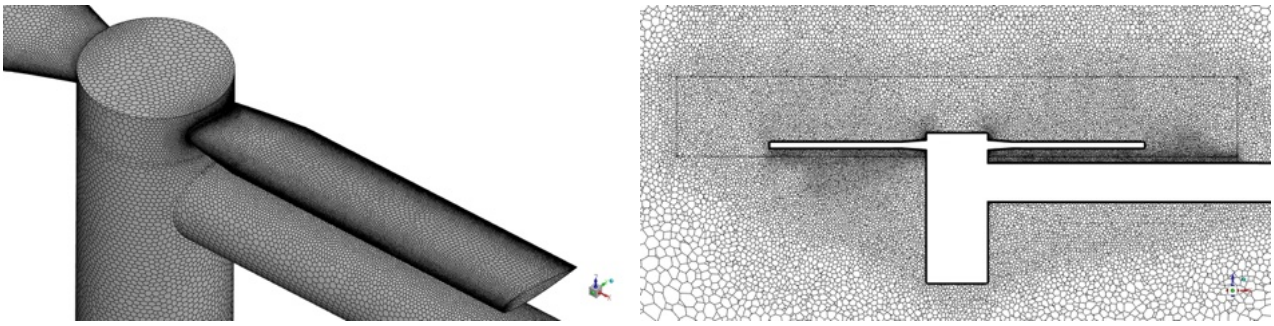

Figure 2: Rotor and beam surface meshes (left) and cut of the mesh along the vertical direction (right) for the rotor RD in interaction with the beam.

Since the flow can be considered incompressible (tip Mach number below 0.25), a segregated solver with constant density is used. Note that the local Reynolds number based on the local blade velocity and chord length increases from about 25.000 at the blade root to 130.000 at the blade tip. The laminar boundary layers is predominant, and fully turbulent URANS simulations are not appropriate with such Reynolds numbers. We therefore used implicit large eddy simulation (implicit LES). Navier-Stokes (N-S) equations are solved directly without turbulence or subgrid scale model and only the largest turbulent structures are resolved. The spatial and temporal discretization schemes are of second order, and the time-step for the implicit unsteady solver is defined to obtain a 1 degree rotation every time-step. The mean and maximal values of the convective Courant number in the rotating part are around 1 and below 10, respectively. Finally, a FW-H analogy has been employed to calculate farfield acoustics based on fluctuating pressure on various surfaces. First, the fluctuating pressure from rotor and beam surfaces is used to compare numerical results with experimental findings. Subsequently, fluctuating pressure from specific elementary surfaces is used to analyze contributions from distinct regions to the overall noise. Note that this approach does not take into account neither convection effects due to local flow velocity, neither diffraction effects of the acoustic waves coming from the rotor on the beam, for instance.

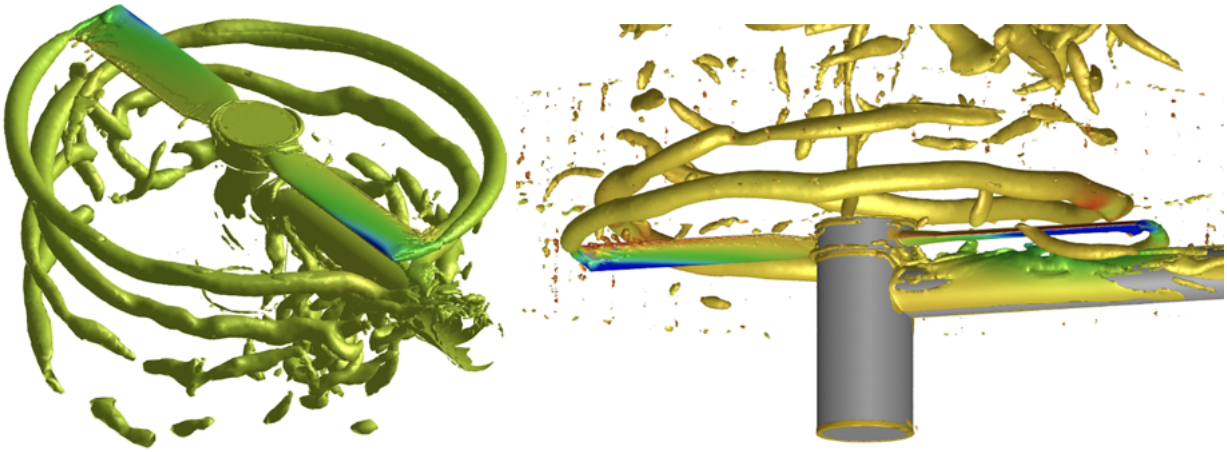

Figure 3: Isocontour of Q criterion ($Q = 10^6 1.s^{-2}$) for the rotor RD (left) and the rotor RU (right).

Simulations for both rotors RD and RU are performed at a rotational speed of 8000 RPM. Corresponding isosurfaces of Q criterion are shown in Figure 3. For the case RD, the tip vortex and

its interaction with the beam downstream are clearly visible. For the case RU, this interaction does not take place anymore, and a detachment on the beam is visible at the passage of a blade.

3. RESULTS

The results are first analyzed in terms of time-averaged thrust and torque Overall, the presence of the beam does not seem to have any influence on the mean thrust and torque, as already seen for similar configurations in a recent paper [21]. The values are about 2.1 N for the thrust and 0.045 N. m-1 for the torque.

3.1. Farfield spectra

The acoustic results of the two configurations are then analyzed. First, experimental farfield spectra at a distance of 1620 mm, latitude angles of $\theta = 0°$ and $\theta = \pm 40°$ with respect to the rotor disk plane and at an azimuth angle of $\phi = 90°$ are plotted in Figure 4. Please note that only the RD rotor is shown without beam, as the results for the rotors RD and RU are almost identical. It was also decided, for the latter azimuthal angle, to compare rotor RU at $\theta = -40°$ with rotor RD at $\theta = +40°$ such that comparison is made at the same angle with respect to the flow direction.

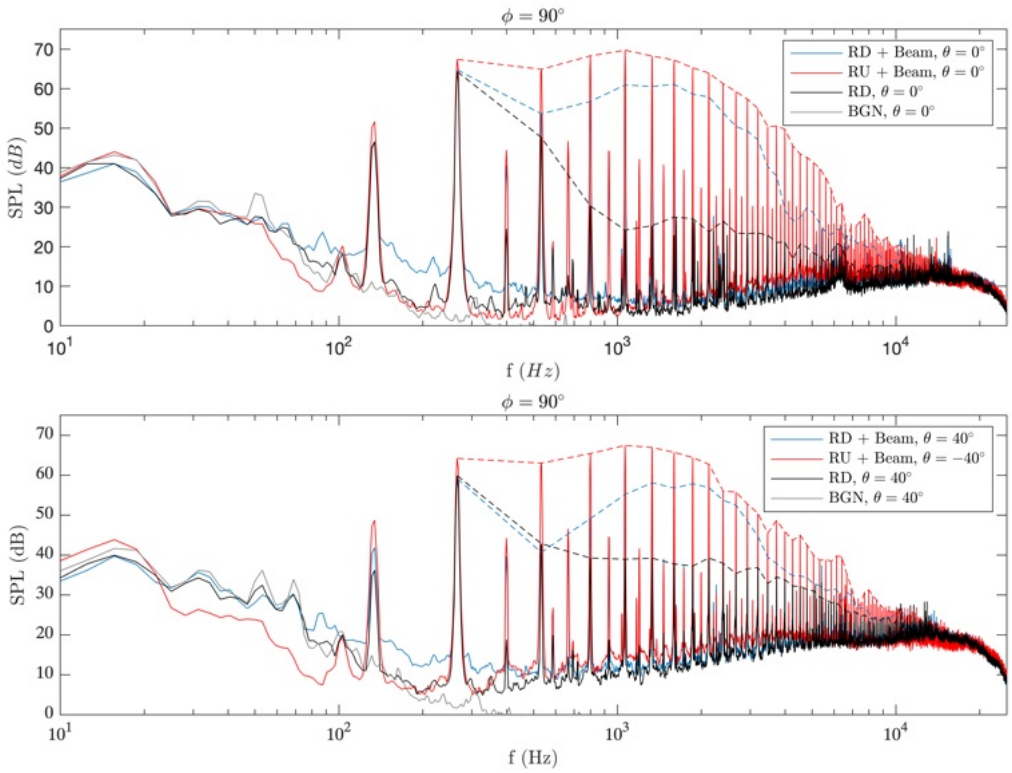

Figure 4: Sound pressure level (SPL) at a latitude angles of $\theta = 0°$ (top) and $\theta = \pm 40°$ (bottom) and at an azimuth angle of $\phi = 90°$ for the two considered configurations.

For the RD rotor in interaction with the beam, similarly to what was observed in previous papers [20, 21], the amplitudes of the BPF, at 266.7 Hz, and of the broadband noise remain unchanged whereas a noticeable increase of the blade passing frequency of up to 30 dB can be observed. For the RU rotor in interaction with the beam, the broadband noise is also unchanged but the amplitude of the BPF and of its harmonics are all increased, with values 5 to 20 dB higher than that obtained for the RU rotor in interaction with the beam.

3.2. Comparison between experimental and numerical results

In order to assess the validity of the acoustical results from the simulations, numerical far field acoustic spectra are compared to experimental amplitudes of the BPF and its harmonics at latitude angles of $\theta = 0°$, and $\theta = 40°$ with respect to the rotor disk plane and at an azimuth angle of $\phi = 90°$ in Figure 5.

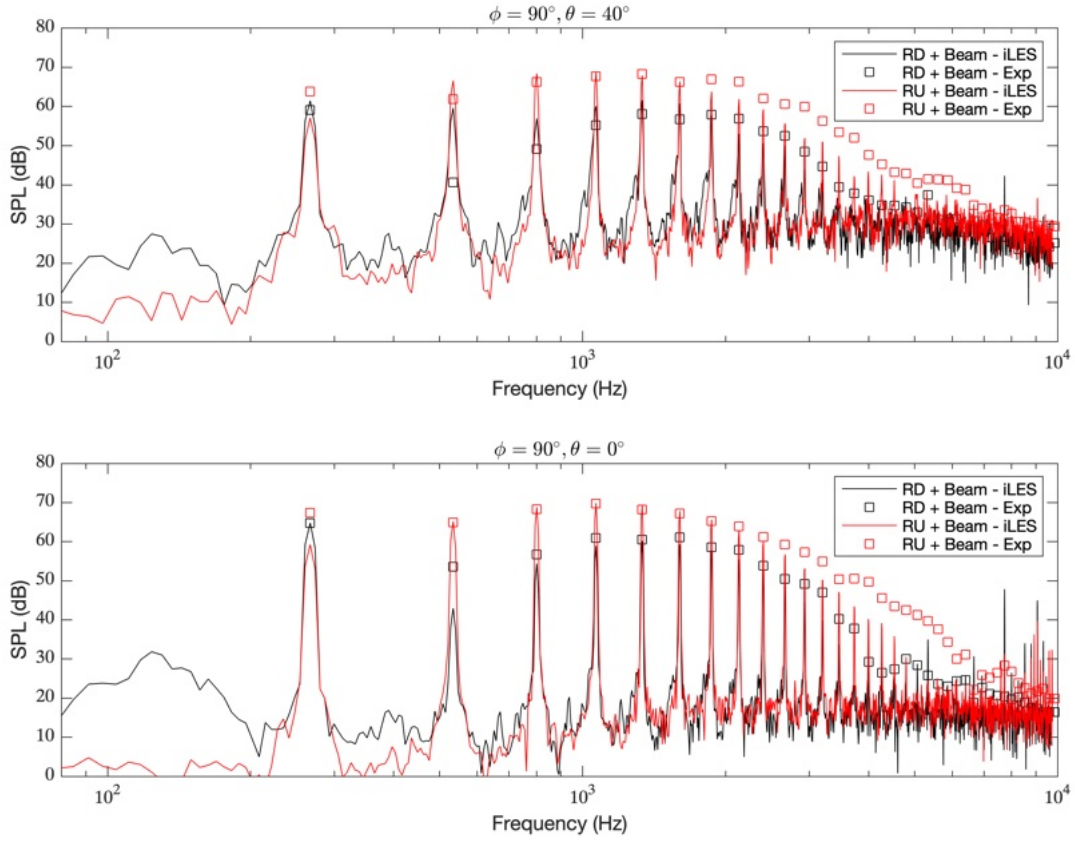

Figure 5: Sound pressure level (SPL) at a latitude angles of $\theta = 40°$ (top) and $\theta = 0°$ (bottom) and at an azimuth angle of $\phi = 90°$ for the rotors RD and RU in interaction with the beam.

Overall, the simulations permit to recover with reasonable accuracy the envelope of the BPF harmonics for the two rotors. Discrepancies are however visible at BPF, 2×BPF, and harmonics ≥ 10×BPF. In particular, results from numerical simulations indicate that the rotor RD generates more noise at the BPF than the rotor RU, which contrasts experimental results where the opposite trend is observed. On the contrary, the amplitude at 2×BPF is well predicted by the simulation of the RU rotor in interaction with the beam while it is overestimated by that of the rotor RD, by up to 20 dB at $\theta = 40°$. Furthermore, the underestimation of high BPF harmonics is related to a lack of accuracy of the simulations in the high frequency range.

Once the numerical results are validated, it is interesting to isolate some elemntary surfaces of the simulation to relate the amplitudes of the BPF and its harmonics to specific components of the setup. The farfield acoustic radiation of the two surfaces assumed to be the main acoustic sources, namely the rotor and the beam, are presented in Figure 6.

Interestingly, the envelope of BPF harmonics appears to be due to the beam radiation only, for both rotors and at both angles $\theta = 0°$ and $40°$. This suggests that, in both cases, the main acoustic source responsible for the envelope of the BPF harmonics is the unsteady loading on the beam due to the rotor passage.

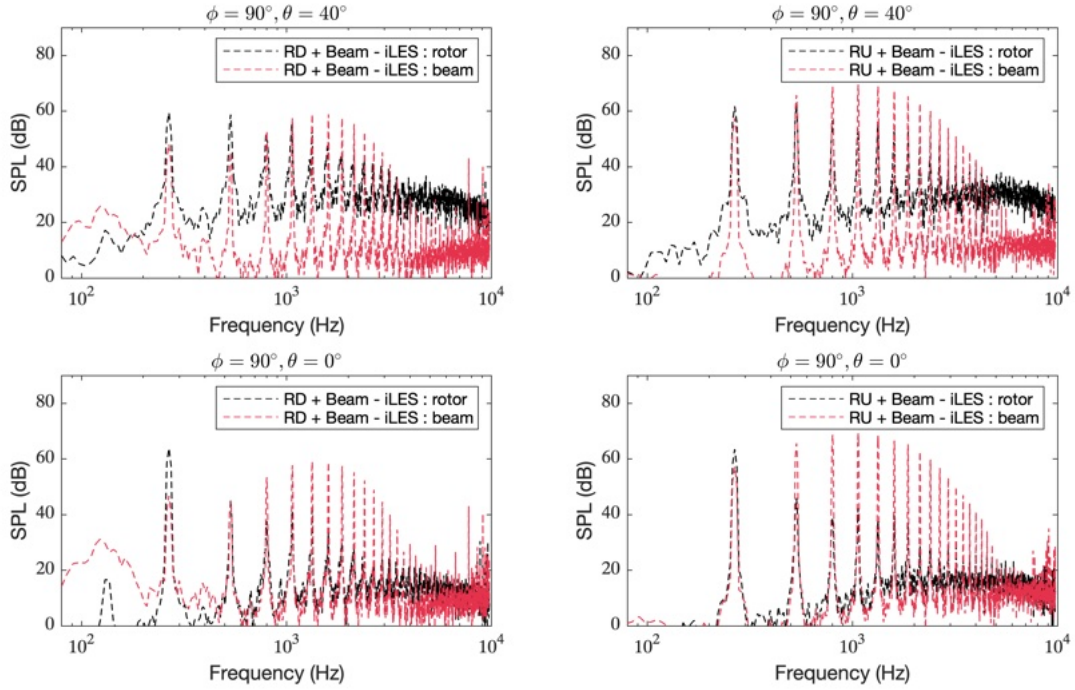

Figure 6: Sound pressure level (SPL) at a latitude angles of $\theta = 40°$ (top) and $\theta = 0°$ (bottom) and at an azimuth angle of $\phi = 90°$ for the rotors RD (left) and RU (right) in interaction with the beam.

3.3. Directivity patterns

In order to study the influence of the beam in a more quantitative way, several specific noise components are analyzed as functions of the directivity angles in Figure 7 : the amplitude of the BPF and its second and fifth harmonics, and the amplitude of the broadband noise. The broadband noise is computed over a frequency range of 1000 Hz < f < 16000 Hz. Please note that tones were cleaned from the spectra before computing the integral value.

For the BPF and the broadband noise, mainly axisymmetric radiation patterns are observed. The BPF presents a maximum level near the rotor disk plane and the broadband noise a minimal amplitude at a latitude angle of $-10°$ for the rotor RD and $+10°$ for the rotor RU. These results are similar to the ones obtained in the case without beam [11]. Those noise sources seem thus not to be affected by the presence of the beam, as already qualitatively observed in Figure 4.

On the contrary, the directivity of the second and fifth harmonics of the BPF seems to be affected by the presence of the beam. For the second harmonic of the BPF, for the rotor RD, non-axisymmetric patterns are noticeable with several minimal amplitudes across the azimuthal direction, at latitude angles $\pm 45°$. For the rotor RU, a dipole like pattern is observed with minimum values at azimuth angles of $0°$ and $180°$ and latitude angle of $0°$. For the fifth harmonic of the BPF, a dipole like pattern is observed with minimum values at azimuth angles of $0°$ and $180°$ and latitude angle of $0°$. The same pattern is observed for all the BPF harmonics which are increasing in the presence of the beam, for both RD and RU rotors.

As the simulations permit to recover rather nicely the envelope of the BPF harmonics, the numerical results are then used to better understand the directivity patterns of the dominant fifth harmonic of the BPF by separating rotor and beam contributions in Figure 8.

This comparison highlights that the dominant fifth harmonic of the BPF is mainly due to radiation coming from the beam, as suggested earlier. Indeed, the simulated beam contribution 3D directivity at the fifth harmonic closely match the experimental 3D directivity, showing that the beam is the main contributor at this frequency.

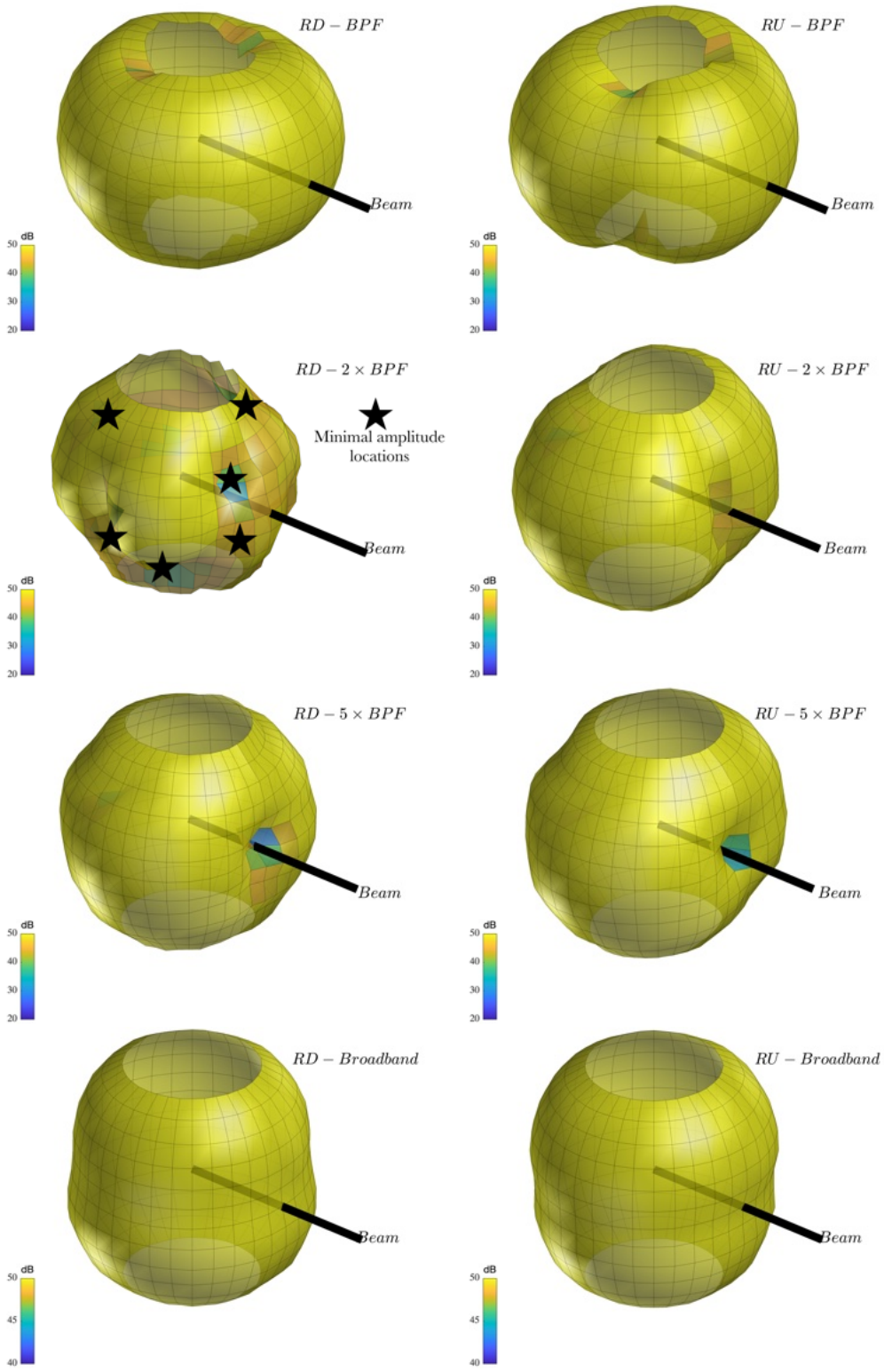

Figure 7: 3D directivity of different noise components measured for the RD rotor (left) and the RU rotor (right) in interaction with the beam : blade passing frequency (BPF), its second and fifth harmonics, and the broadband noise.

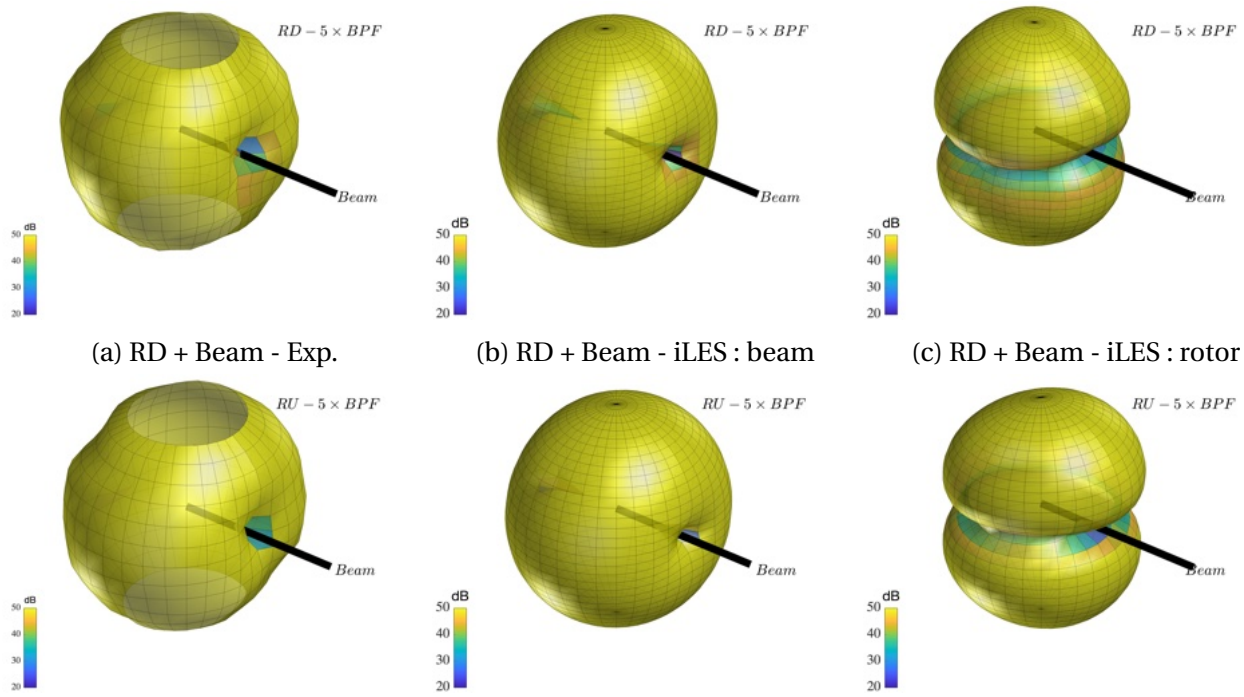

(a) RD + Beam - Exp. (b) RD + Beam - iLES : beam (c) RD + Beam - iLES : rotor

(d) RU + Beam - Exp. (e) RU + Beam - iLES : beam (f) RU + Beam - iLES : rotor

Figure 8: 3D directivity of the fifth blade passing frequency (BPF) harmonic for the RD rotor (top) and the RU rotor (bottom) in interaction with the beam : measured (left), simulated beam contribution (center) and simulated rotor contribution (right).

4. ANALYTICAL MODELING - BEAM UNSTEADY LOADING NOISE

As the main acoustic mechanism creating BPF harmonics seems to be the unsteady loading on the beam for both RD and RU rotors, the model proposed by Wu et al. [13] is tested. In this model, in a similar way as in strip theory, a rotor blade section located at a radius r is represented as a line vortex with circulation determined by the steady loading of the blade. This circulation, which can be considered quasi-steady, interacts with the potential flow around a two-dimensional cylinder, namely the cylindrical beam. Thus, the interaction problem can be seen as a two-dimensional incompressible potential flow problem, resulting in a beam-potential interaction model. Thanks to this model, the unsteady loading at the beam surface can be reconstructed. Then, the unsteady load acting on the beam is computed and Hanson model [23] is used to propagate this unsteady loading on the beam to the far field. This model has been implemented and validated recently in Vella et al. [24]. Entries necessaries include notably induced velocity at the beam location, taken here from an implicit LES simulation of a rotor without beam, and load distribution (thrust and torque) of the blade along the radius. More details can be found in Vella et al. [24].

First, 3D directivities at $5 \times BPF$ are plotted in Figure 9 for the RD and RU rotors in interaction with the beam. It can be seen that the overall directivities match very well the experimental and numerical directivities found before at $5 \times BPF$, in Figures 7 and 8.

In order to be more quantitative, the amplitudes at BPF harmonics found by the model are compared with experimental and numerical results at an azimuth angle of $\phi = 90°$ and at latitude angles of $\theta = 40°$ and $\theta = 0°$, in Figure 10.

Looking at the harmonics of the BPF for which the noise source due to the unsteady loading on the beam is supposed to be dominant from the numerical simulation, the results are in rather good agreement with experimental and numerical results for the rotor RD in interaction with the beam, but it is not the case for the rotor RU in interaction with the beam. Another mechanism is

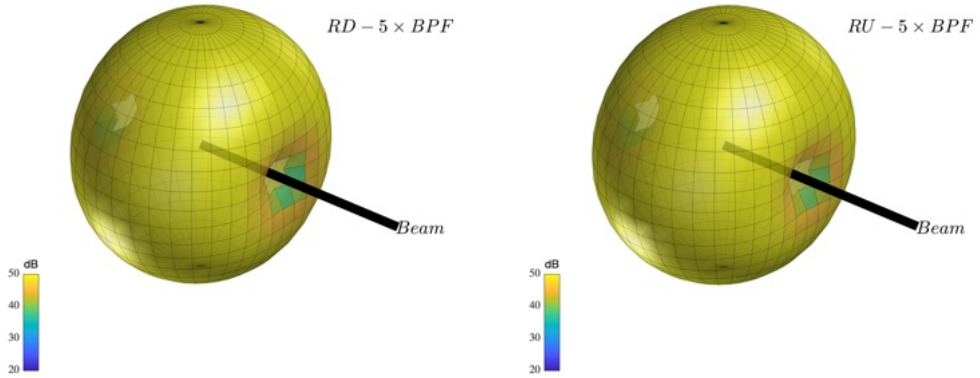

(a) RD + Beam - Model (b) RU + Beam - Model

Figure 9: 3D directivity from Wu's analytical model of the RD (left) and RU (right) rotors fifth blade passing frequency (BPF) harmonic in interaction with the beam.

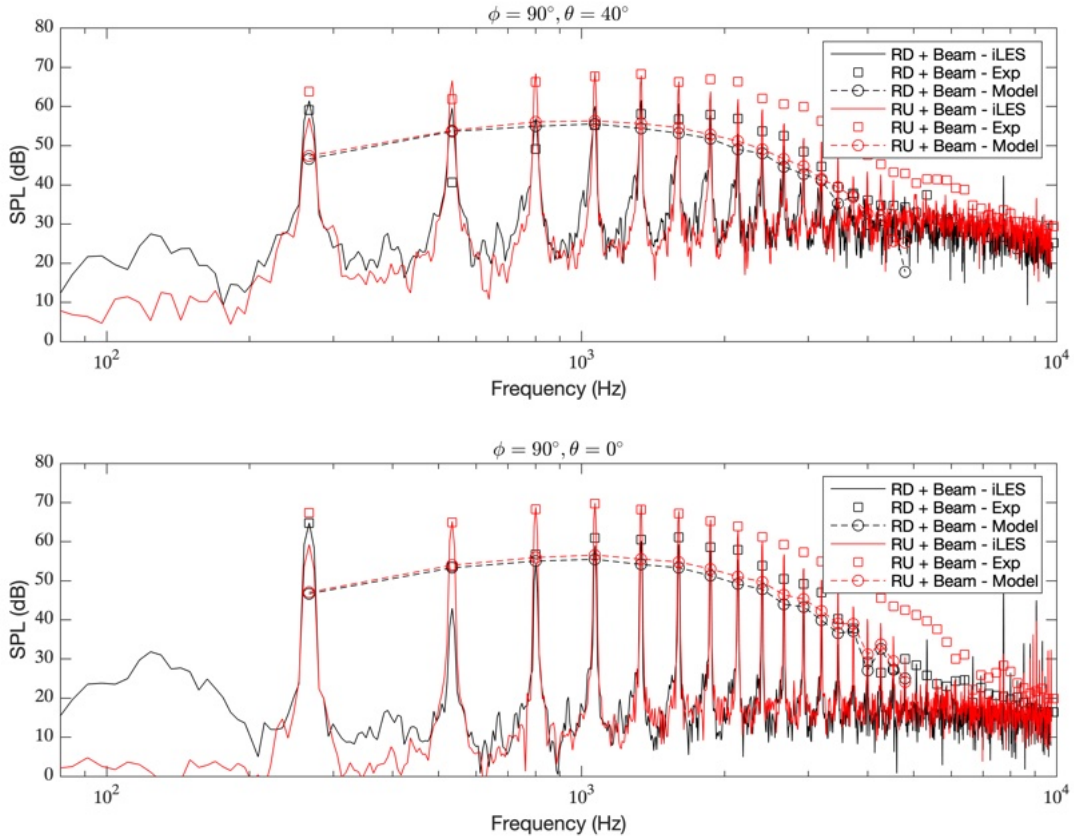

Figure 10: Sound pressure level (SPL) at a latitude angles of $\theta = 40°$ (top) and $\theta = 0°$ (bottom) and at an azimuth angle of $\phi = 90°$ for the rotors RD and RU in interaction with the beam; comparison between experiments, simulations and model.

thus at play for the RU rotor in interaction with the beam. This could be linked to periodic flow separation on the beam when the blade is passing nearby, as observed in Figure 3. This possible flow separation is not taken into account in the potential interaction model, and could explain the discrepancies between the model and the numerical and experimental results for the RU rotor in interaction with the beam.

5. FINAL COMMENTS AND CONCLUSIONS

The radiation characteristics of rotors are studied experimentally and numerically for two low Reynolds number, two-bladed small-scale rotors in interaction with a cylindrical beam. Those two rotors have a different pitch orientation which allows to produce an airflow in the direction of (RD rotor) or away from (RU rotor) the beam. The rotor-beam airflow interaction does not have any significant impact on aerodynamic loads. In terms of acoustics, the presence of the beam does not seem to affect the blade passing frequency (BPF) and the broadband noise sound pressure levels (SPL) radiation patterns. However, the beam significantly increases (up to 30 dB for the RU rotor) the BPF harmonics 2×BPF to 15×BPF SPL with a highest SPL for BPF harmonics typically between 5×BPF and 6×BPF. The most intense BPF harmonics exhibits a horizontal dipole-like radiation pattern aligned with the beam axis. The experimental campaign allows also to assess the reliability of the proposed coupled implicit LES / FW-H approach, which is validated for the dominant BPF harmonics. This allows to use the ability of numerical simulations to predict the radiated acoustic field related to elementary parts of the setup in order to discriminate the noise contributions. Interestingly, the level increase and the characteristic directivity pattern of the dominant BPF harmonics are related to the unsteady loading on the beam for both configurations. An analytical modeling proposed in the literature and based on Wu and Hanson models for this noise source mechanism is finally compared for both configurations. The results are in good agreement with experimental and numerical results for the rotor RD in interaction with the beam, but it is not the case for the rotor RU in interaction with the beam which suggests that an additional noise source mechanism is taking place in the later case. This will be studied in the future.

ACKNOWLEDGEMENTS

The authors gratefully acknowledge financial support from the DGA. They are grateful to the entire ISAE-SUPAERO technical team for the success of the experimental campaign. The numerical part of this work was performed using resources from GENCI [CCRT-CINES-IDRIS] (Grant 2023-[A0142A07178]). The authors thank Michel Roger for his insights and advices.

REFERENCES

1. L Gutin. On the sound field of a rotating propeller. *Physikalische Zeitschrit der Sowjetinion: Physical magazine of the Soviet Union volume 9 number 1*, 9(NACA-TM-1195), 1948.
2. JE Ffowcs Williams and DL Hawkings. Theory relating to the noise of rotating machinery. *Journal of Sound and Vibration*, 10(1):10–21, 1969.
3. A.R. George. Helicopter noise: State-of-the-art. *Journal of Aircraft*, 15(11):707–715, 1978.
4. K.S. Brentner and F. Farassat. Helicopter noise prediction: the current status and future direction. *Journal of Sound and Vibration*, 170(1):79–96, 1994.
5. N.S. Zawodny, D.D. Boyd Jr, and C.L. Burley. Acoustic characterization and prediction of representative, small-scale rotary-wing unmanned aircraft system components. In *AHS 72nd Annual Forum*, 2016.
6. Y. Jo, T. Jardin, R. Gojon, M.C. Jacob, and J.M. Moschetta. Prediction of noise from low Reynolds number rotors with different number of blades using a non-linear vortex lattice method. In *25th AIAA/CEAS Aeroacoustics Conference*, page 2615, 2019.

7. R. Serré, H. Fournier, and J.M. Moschetta. A design methodology for quiet and long endurance MAV rotors. *International Journal of Micro Air Vehicles*, 11, 2019.
8. R. Serré, N. Gourdain, T. Jardin, M.C. Jacob, and J.M. Moschetta. Towards silent micro-air vehicles: optimization of a low Reynolds number rotor in hover. *International Journal of Aeroacoustics*, 18(8):690–710, 2019.
9. E. Grande, G. Romani, D. Ragni, F. Avallone, and D. Casalino. Aeroacoustic investigation of a propeller operating at low reynolds numbers. *AIAA Journal*, pages 1–12, 2021.
10. G. Romani, E. Grande, F. Avallone, D. Ragni, and D. Casalino. Performance and noise prediction of low-reynolds number propellers using the lattice-boltzmann method. *Aerospace Science and Technology*, page 107086, 2021.
11. R. Gojon, T. Jardin, and H. Parisot-Dupuis. Experimental investigation of low reynolds number rotor noise. *The Journal of the Acoustical Society of America*, 149(6):3813–3829, 2021.
12. N.S. Zawodny and D.D. Boyd Jr. Investigation of rotor-airframe interaction noise associated with small-scale rotary-wing unmanned aircraft systems. In *AHS 73rd Annual Forum*, 2017.
13. Y. Wu, M.J. Kingan, and S.T. Go. Propeller-strut interaction tone noise. *Physics of Fluids*, 34(5):055116, 2022.
14. Michel Roger, Daniel Acevedo-Giraldo, and Marc C Jacob. Acoustic versus aerodynamic installation effects on a generic propeller-driven flying architecture. *International Journal of Aeroacoustics*, 21(5-7):585–609, 2022.
15. B. Cotte, T. Rigall, and C. Deora. Experimental characterization and analytical modelling of rotor tonal noise. In *Forum Acusticum*, pages 2937–2943, 2020.
16. N. Intaratep, W.N. Alexander, W.J. Devenport, S.M. Grace, and A. Dropkin. Experimental study of quadcopter acoustics and performance at static thrust conditions. In *22nd AIAA/CEAS Aeroacoustics Conference*, page 2873, 2016.
17. S. Yoon, P.V. Diaz, D.D. Boyd Jr, W.M. Chan, and C.R. Theodore. Computational aerodynamic modeling of small quadcopter vehicles. In *AHS 73rd Annual Forum*, 2017.
18. C.E. Tinney and J. Sirohi. Multirotor drone noise at static thrust. *AIAA Journal*, 56(7):2816–2826, 2018.
19. H. Lee and D.J. Lee. Rotor interactional effects on aerodynamic and noise characteristics of a small multirotor unmanned aerial vehicle. *Physics of Fluids*, 32(4):047107, 2020.
20. R. Gojon, N. Doué, H. Parisot-Dupuis, B. Mellot, and T. Jardin. Aeroacoustic radiation of a low reynolds number two-bladed rotor in interaction with a cylindrical beam. In *28th AIAA/CEAS Aeroacoustics 2022 Conference*, page 2972, 2022.
21. R. Gojon, H. Parisot-Dupuis, B. Mellot, and T. Jardin. Aeroacoustic radiation of low reynolds number rotors in interaction with beams. *The Journal of the Acoustical Society of America*, 154(2):1248–1260, 2023.
22. T. Jardin, R. Gojon, N. Doué, and H. Parisot-Dupuis. Numerical and experimental analysis of the influence of solidity on rotor aeroacoustics at low reynolds numbers. *International Journal of Aeroacoustics*, 22(1-2):85–109, 2023.
23. D. B. Hanson and D. J. Parzych. Theory for noise of propellers in angular inflow with parametric studies and experimental verification. *NASA Contractor Report 4499*, 1993.
24. E. Vella, R. Gojon, H. Parisot-Dupuis, N. Doué, T. Jardin, and Roger M. Mutual interaction noise in rotor-beam configuration. In *30th AIAA/CEAS Aeroacoustics 2024 Conference*, 2024.